

Ludwig-Maximilians-Universität München
Physik B.Sc.

Exakte Lösungen von Dimer-Modellen auf dem Dreiecksgitter

Bachelorarbeit
Yuhao Zhao



24.07.2017

Betreuer:

Prof. Dr. Matthias Punk

Ludwig-Maximilians-Universität München
Physics B.Sc.

Exact Solutions of Dimer Models on the Triangular Lattice

Bachelor Thesis
Yuhao Zhao



24.07.2017

Supervisor:

Prof. Dr. Matthias Punk

Acknowledgement

I would like to express my sincere gratitude to my supervisor Prof. Dr. Matthias Punk for giving me the opportunity to write my bachelor thesis with him. He guided me into this intriguing topic with great patience and kindness. I really appreciate his instructive mentoring.

Thanks also to my friend Chao Wan for improving and polishing the English expressions in this article.

Contents

1	Introduction	3
2	Model	6
2.1	RK-Model	6
2.2	Hilbert space	7
2.3	Fermionic dimer	8
3	Quantum dimer model on triangular lattice	10
3.1	The dimer model on triangular lattice	10
3.1.1	Rokhsar-Kivelson quantum dimer Hamiltonian	10
3.1.2	Hamiltonian with doped fermionic dimers	11
3.2	Exact ground states	13
3.2.1	Two doped fermionic dimers state	14
3.2.2	Plaquette states	14
3.2.3	Exact ground state	15
3.3	Perturbations around RK line	20
4	Summary	23

1 Introduction

Decades ago, superconductive phenomena have been observed in a rather unexpected material, a transition metal oxide.[1] This unusual discovery motivated tremendous researches to explain the mechanism behind the presence of superconductivity. See Fig.(1). An extremely intriguing phase region with remarkable behaviours is located at low hole-doping, between the Mott insulator at half filling and the superconducting phase. Use a variety of different experimental techniques, which enabled more and more refined measurement, this region has been classified as a so-called pseudogap (PG) phase.

This hole-doped system is generated from a parent Cu-based compound, which is known as an antiferromagnetic (AF) insulator. As the charge carriers are doped (holes in our case) into the parent compound, the AF state is destroyed and superconductivity (SC) emerges below a critical temperature. It is believed that a comprehension of the intermediate area between AF and SC state plays a crucial role for understanding the physics in hope-doped cuprates, experiments are thus carried out to characterize this so-called PG phase and to determine its properties. It turns out that the spin susceptibility drops at low temperatures before the onset of superconductivity, which is referred to the formation of a spin structure with lower degree of freedom.[2] Moreover, the specific heat of the system decreases linearly below room temperature, and shows a jump at the critical temperature where the material undergoes a superconducting transition. This jump of the specific heat, however, weakens with lower doping densities. Thus, the spins there should undergo a binding process that their entropy can be gradually reduced.[3][4][5] Decades prior to these experimental uncovers, theories anticipated that a pair of spins can bind into a singlet bond in low doped system, describing the behaviours of specific heat above. Anderson first introduced this ideal in his well known resonating valence bond (RVB) model; Rokhsar and Kivelson later followed in this direction and established the RK-model. We would give a brief introduction about these historical works in Sec.(2.1).

More remarkable properties of PG metal are found in recent experimental progresses.

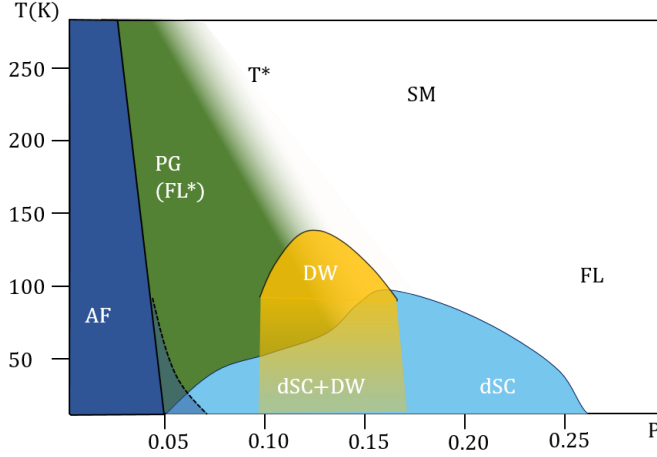


Figure 1: Schematic phase diagram of hole-doped cuprates as function of doping p and temperature T . At around $p = 0$ the cuprate compound behaves as an antiferromagnetic insulator. Upon doping away from the insulating phase, the PG phase is present in the temperature interval $T_c < T < T^*$, while the superconductivity emerges at temperature below T_c . Figure adapted from [6].

One of them shows a mysterious open Fermi arc in the spectrum through angle resolved photoemission spectroscopy (ARPES), where a large closed Fermi surface is expected according to the Luttinger theorem.[7][5][8] Furthermore, Hall measurement reports p as the density of charge carriers in the system, rather than the larger $1 + p$ relative to a fullfilled band.[9][10] This also provides an alternative perspective that the suppression of Drude weight in early experiments is related to a reduced density of charge carriers, rather than a suppressed kinetic term.[5][11] The above mentioned RVB model, however, failed in describing these observations. Nonetheless, a fractionalized Fermi liquid (FL*) model is proposed by Senthil, Schdev and Vojta based on RVB picture, assigning the violation of Luttinger theorem to the appearance of topological order[12]. Punk, Allais and Sachdev then employed this account to construct a new dimer model where the PG metal is interpreted as a finite temperature realization of FL*. They show in [6] that the key features of PG metal are well described by this model.

Along this route, Johannes Feldmeier provides in [13] an exact ground state solution of this new dimer model on the square lattice; perturbs it in the parameter space and a FL* structure can be recognized. In this article, we intend to generalize this model

further onto the triangular lattice, which is usually seen as a tilted square lattice with additional diagonal link. We can see these connections between them from our results that they can recover the results of the square lattice case in spite of the additional orientation. As a conclusion, we confirm that a FL* like ground state can be expected in the triangular lattice.

2 Model

2.1 RK-Model

Forty years ago, Rokhsar and Kivelson developed the RK-Model[14], intending to explain the physics of an antiferromagnetic (AF) Mott insulator doped with mobile charge carriers along the route provided by Anderson with his resonating valence bond (RVB) model[15]. In Mott insulator, electrons are believed to be locked at their own site with anti-parallel aligned spins due to strong effects. In this case, the energy cost to fulfill a site with two electrons U dominates compared to the hopping energy t , and the needed exchange energy J for two parallel aligning spins is given by $4t^2/U$, which leads to an energetically favorable AF state. The simplest way to capture these properties is employing the well-known $t - J$ model, which is viewed as the strong coupling limit of Hubbard model. [5] However, with the increasing density of the doped hole, the unoccupied charge carriers strongly stimulate the hopping of spins so that the AF state as well as its insulativity is destroyed. The system becomes consequently frustrated and its structure is determined by the competition of the t and J . The original RVB model then suggests that by forming singlet bonds, spins become energetically more competitive with the enduring anti-parallel structure, and in the low doped limit, the doped holes can move in this singlet background without breaking bonds so that the AF state consists.


The RVB model can be further qualitatively classified into two sorts. One is so-called short-range resonating valence bond (SR-RVB) model developed by Kivelson, Rokhsar and Sethne in year 1977. The range of the valence bonds are restricted within the nearest neighbors in this model, while the amplitudes of the long range valence bands are expected to decay exponentially.[16] One year later, in their article [14], Rokhsar and Kivelson proposed the famous RK quantum dimer model, where the exponentially decaying spin-spin correlations finally leads to a sufficiently large spin gap. Thus, a manifold of low-energy states spanned by the linearly independent set of nearest-neighbor valence-bond states can be considered. In other words, they argued that the effective short-range dimer Hamiltonian in fact agrees with that of valence-bond states despite

the nonorthogonality. Punk, Allais and Schadev later employed this QDM model in their article [6], and expanded that by introducing a new specie of dimers. They offered in this way an alternative perspective to explain the mechanism behind the appearance and the behaviours of PG state in the low doped cuprate.

2.2 Hilbert space

As mentioned above, the Hilbert space of the original QDM model on square lattice is spanned by the orthonormal states $|C\rangle$, where each C represents a specific dimer configuration. The configurations have to satisfy the hard-core constraint, namely each spin only binds once with one nearest neighbor at the same time. Hence, a dimer is composed of a pair of spins bound in singlet state. We introduce the bosonic dimer operator D to represent it:

$$\frac{1}{\sqrt{2}}(c_{i,\uparrow}^\dagger c_{i+\hat{\eta},\downarrow}^\dagger - c_{i,\downarrow}^\dagger c_{i+\hat{\eta},\uparrow}^\dagger) |0\rangle \rightarrow D_{i,\eta}^\dagger |0\rangle, \quad (1)$$

where $c_{i,\uparrow}^\dagger$ creates a spin-up electron on the site i as $c_{i+\hat{\eta},\downarrow}^\dagger$ stands for its bound spin-down electron on site $i + \hat{\eta}$ as $\eta \in \{x, y\}$. Visually, we draw an orange ellipse covering two sites  for illustration, and the Hamiltonian of QDM model is written as:

$$H_{RK} = \sum_{\text{plaquettes}} [-J(|\langle \text{orange ellipse} \rangle\rangle\rangle \langle \langle \text{orange ellipse} | + H.c.) + V(|\langle \text{orange ellipse} \rangle\rangle \langle \langle \text{orange ellipse} | + |\langle \text{orange ellipse} \rangle\rangle \langle \langle \text{orange ellipse} |)] \quad (2)$$

with this notation. The first term with a prefactor J is a kinetic term that describes the resonance between parallel nearest-neighbor dimers within a plaquette; the second term with the prefactor V , like the energy offset U in Hubbard model, describes the repulsion between them. Note that J and V here are both positive. This choice is purely conventional on square lattice[14], and remains the same for the triangular lattice[17]. Analogous to the $t - J$ model, the competition between J and V determines the ground states of Hamiltonian H_{RK} . For $V > J > 0$, the so-called valence-bond solid (VBS) states serve as the only ground states, where the dimers become "staggered" as the parallel aligning is energetically not favorable, see Fig.(2) On contrary, for $J > 0 > V$, the number of flippable plaquettes is maximized, leading to a "column state". Rokhsar and Kivelson then stated that the Hamiltonian can be exact solvable at the middle

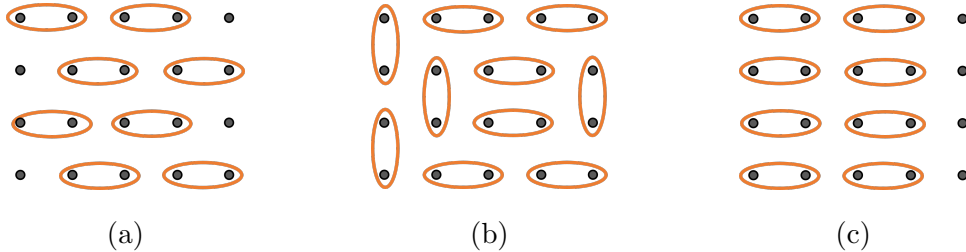


Figure 2: (a) a staggered state for $V > J$. (c) the column state. (b) a typical dimer covering on square lattice.

point $J = V$, namely "RK-point", where the unique zero-energy ground state ψ_0 is composed by the equal-amplitude superposition $\sum_C |C\rangle$. [14]

We later need to generalize this model onto the triangular lattice for further calculations. One of the most important points is the orthogonality of the basis vectors. The short-range effective Hamiltonian Eq.(2) corresponds to the case despite the nonorthogonality of the valence-bond states on square lattice [14]. We hope this is the case on the triangular lattice as well. Fortunately, by evaluating the overlap matrix, for the sufficiently large triangular lattice, the overlap becomes eventually very small though never zero. [18] Thus, as the tiny overlap among configurations $\{|C\rangle\}$ is neglected, $\{|C\rangle\}$ is taken as a set of complete orthonormal basis for short-range dimer Hamiltonian on the triangular lattice, and a Hamiltonian based on orthonormal dimer configurations is now allowed to be built on the triangular lattice. We will show it in details in Sec.(3)

2.3 Fermionic dimer

We reviewed in the previous sections the establishment of QDM model and its properties. However, we can only describe dope-less cuprates with the QDM model consisting of pure bosonic dimers. In this section, we proceed to see how doped holes are treated in the models, and arrive at the expanded dimer model introduced in [6].

As holes are doped with sufficiently large density into a short-range RVB state, the singlet bonds can be broken. Its debris is classified into two types. The piece carrying charge $+e$ but no spin is called "holon", while "spinon" stands for the other type with no charge but spin $1/2$. They actually are believed to move in principle separately

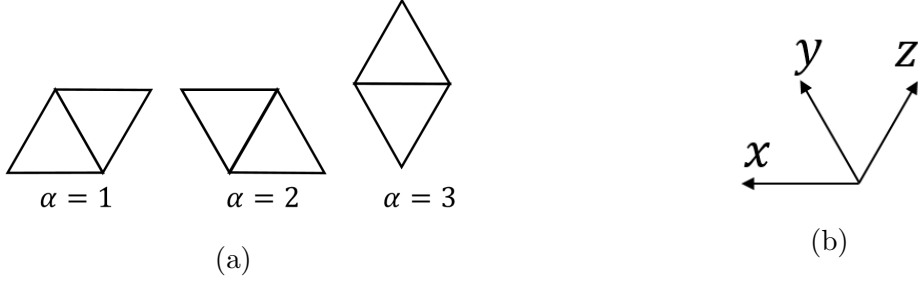


Figure 3: (a) Orientations are denoted with $\alpha = 1, 2, 3$ (b) Coordinate we used in calculation on the triangular lattice.

on the lattice at RK-point, and are therefore regarded as deconfined monomers in the 2D-QDM model.[17]

In [6], the authors treat these monomers, however, together by introducing new specie of dimer, which is a monomer bond formed by a pair of neighbouring spinon and holon. They show that, in a hole-doped antiferromagnet, the presence of such dimers explains the unexpected hole density p in the system. This new dimer has the expression

$$F_{i,\eta,s}^\dagger |0\rangle \rightarrow \frac{1}{\sqrt{2}}(c_{i,s}^\dagger + c_{i+\hat{\eta},s}^\dagger) |0\rangle, \quad (3)$$

and is named as fermionic dimer for its half-integer spin (in our case, $s = 1/2$, carried by the spinon). Note that since the holon and spinon are deconfined at RK-point, this combination is regarded as a result of energetic preference, i.e., a short-range attraction. The low energy Hilbert space of the QDM model hence needs to be expanded to adapt to this introduction of fermionic dimer, and it is simply accomplished by adding doped fermionic dimer into hard-core coverings.

3 Quantum dimer model on triangular lattice

In this section we build up the corresponding Hamiltonian to describe the interactions between doped hole and its neighboring spins on the triangular lattice by implementing the quantum dimer model. Then with the method developed by Rokhsar and Kivelson of choosing a line in parameter space to reconstruct the Quantum dimer Hamiltonian as a sum of local projectors [14], we are able to obtain the exact ground state wave functions. Finally, we study the perturbations around the chosen parameter line, and are able to see that the small perturbations leading to a thorough reconstruction of flat dispersion relation of the ground state, as well as to the presence of Fermi pockets.

We follow in this section the calculations of exact ground state and perturbations around RK line on square lattice done by J.Feldmeier in [13], and expand to the triangular lattice case.

3.1 The dimer model on triangular lattice

3.1.1 Rokhsar-Kivelson quantum dimer Hamiltonian

In order to represent all configurations of dimers on a triangular lattice, we use elementary plaquettes that are parallelograms consisting of an up- and down triangle. One attention should be made here is that unlike all plaquettes on the square lattice aligned in the same direction in [13], they have three possible orientations on the triangular lattice, namely ∇ rotated by $\pm 60^\circ$ [19]. Thus, we construct the Rokhsar-Kivelson quantum dimer Hamiltonian:

$$\hat{H}_{RK} = -J\hat{T} + V\hat{V} = \sum_i \sum_{\alpha=1}^3 (-J |\text{triangle}_\alpha\rangle \langle \text{triangle}_\alpha| + H.c.) + V (|\text{triangle}_1\rangle \langle \text{triangle}_1| + |\text{triangle}_2\rangle \langle \text{triangle}_2| + |\text{triangle}_3\rangle \langle \text{triangle}_3|), \quad (4)$$

where the sum on α runs over the three orientations of plaquettes, and i represents the site on triangular lattice. (For the definition of orientation index α and coordinate we chose see in Fig.(3)) What would happen to the ground state now when we vary the balance of V and J ? We see that, in the square lattice the spins will undergo a phase transition from VBS to a spin liquid (RVB) state, and this is roughly the the case on

the triangular lattice. See Fig.(4). However, unlike the $U(1)$ spin liquid on the square

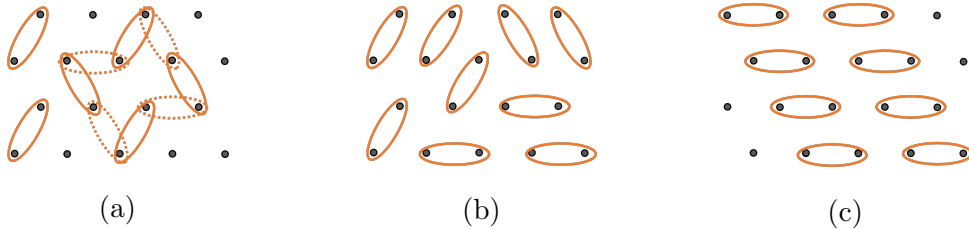


Figure 4: (b) a typical RVB dimer covering on the triangular lattice. (c) the column state. (a) A staggered state with the four-dimer move connecting it to other states. In this staggered configuration a local dimer dynamics is shown.[19]

lattice, the Z_2 RVB liquid (Fig.(4)(b)) can stay in a stable state over a parameter regime around the special RK-point $J = V$, [18] implies a more stable ground state of QDM on the square lattice when the next near neighbors are taken in concern.

3.1.2 Hamiltonian with doped fermionic dimers

In [6], Punk, Allais and Sachdev detailed the Hamiltonian introduced by doped fermionic dimers on the square lattice. Similarly, we use the following results to describe the Hamiltonian of plaquettes with certain orientation

$$H = \sum_{\alpha}^3 H_{\alpha} \quad , \text{with} \quad H_{\alpha} = H_{RK,\alpha} + H_{1,\alpha} + H_{\nu_1,\alpha} \quad , \quad (5)$$

Note that in the Hamiltonian above, we treated different orientations separately. Its validity is endowed by the property that the dimers in different orientations are mutually independent in terms of the Hamiltonian, so that each Hamiltonian is merely related to the parallel plaquettes, i.e., within one orientation. Moreover, if there is no dimer appearing diagonally in the parallelogram plaquettes, the Hamiltonian should be similar to that of the square lattice, since the parallelogram is merely a tilted square. This can be seen from the following calculations.

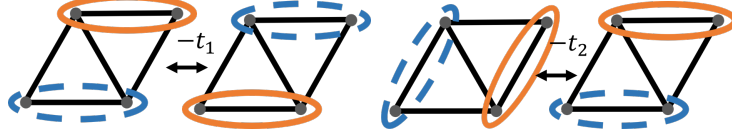


Figure 5: Hoppings of fermionic dimer (blue, dashed) and bosonic dimer (orange) on a plaquette with certain orientation ($\alpha = 1$).

The second term of the Hamiltonian for $\alpha = 1$ is

$$\begin{aligned}
H_{1,\alpha=1} = & -t_1 \sum_i (F_{i,x}^\dagger D_{i+z,x}^\dagger D_{i,x} F_{i+z,x} + D_{i,x}^\dagger F_{i+z,x}^\dagger F_{i,x} D_{i+z,x} \\
& + F_{i,z}^\dagger D_{i+x,z}^\dagger D_{i,z} F_{i+x,z} + D_{i,z}^\dagger F_{i+x,z}^\dagger F_{i,z} D_{i+x,z}) \\
& - t_2 \sum_i (F_{i,x}^\dagger D_{i+z,x}^\dagger D_{i+x,z} F_{i,z} + F_{i,x}^\dagger D_{i+z,x}^\dagger D_{i,z} F_{i+x,z} \\
& + D_{i,x}^\dagger F_{i+z,x}^\dagger F_{i+x,z} D_{i,z} + D_{i,x}^\dagger F_{i+z,x}^\dagger F_{i,z} D_{i+x,z} \\
& + D_{i,z}^\dagger F_{i+x,z}^\dagger F_{i+z,x} D_{i,x} + D_{i,z}^\dagger F_{i+x,z}^\dagger F_{i,x} D_{i+z,x} \\
& + F_{i,z}^\dagger D_{i+x,z}^\dagger D_{i+z,x} F_{i,x} + F_{i,z}^\dagger D_{i+x,z}^\dagger D_{i,x} F_{i+z,x}),
\end{aligned} \tag{6}$$

where t_i represents amplitude of energy contributions of two selected short-range hoppings of fermionic dimers, which are illustrated in Fig.(5). Other short-range as well as long-range hoppings are not prohibited in our model, however, we are allowed to omit them to simplify the calculation since their amplitudes are expected to decay exponentially with increasing distance.

The explicit calculation of t_i through the perturbative mapping can be found in the Appendix of [6].

The third term H_{ν_1} in Eq.(5) indicates the energy contribution of flippable plaquettes which contain doped fermionic dimers. With the characterizing amplitude parameter ν_1 , the corresponding term H_{ν_1} for $\alpha = 1$ is

$$\begin{aligned}
H_{\nu_1,\alpha=1} = & \nu_1 \sum_i (F_{i,x}^\dagger D_{i+z,x}^\dagger D_{i+z,x} F_{i,x} + D_{i,x}^\dagger F_{i+z,x}^\dagger F_{i+z,x} D_{i,x} \\
& + F_{i,z}^\dagger D_{i+x,z}^\dagger D_{i+x,z} F_{i,z} + D_{i,z}^\dagger F_{i+x,z}^\dagger F_{i+x,z} D_{i,z}) .
\end{aligned} \tag{7}$$

To further evaluate the exact ground state wave functions, a line in parameter space

needs to be identified, where the Hamiltonian from Eq.(5) can be reconstructed as a sum of projectors.[14] The choice in determining the original RK Hamiltonian is a point $J = V$ for only two parameters, namely RK point. Similarly, we take the choice

$$\nu_1 = t_2 = -t_1, \quad (8)$$

and insert this RK-line into Eq.(5). We obtain

$$\begin{aligned}
H = J \sum_l \sum_{\alpha}^3 (|\text{triangle}\rangle - |\text{triangle}\rangle)(\langle \text{triangle} | - \langle \text{triangle} |) + \\
+ \nu_1 \sum_l \sum_{\alpha}^3 (|\text{triangle}\rangle + |\text{triangle}\rangle - |\text{triangle}\rangle - |\text{triangle}\rangle)(\langle \text{triangle} | + \langle \text{triangle} | - \langle \text{triangle} | - \langle \text{triangle} |).
\end{aligned} \quad (9)$$

The first term represents the original RK Hamiltonian on the triangular lattice while the second one describes the Hamiltonian produced by introduced fermionic dimers. Their similar forms guide us to the following conjecture: As in the original RK RVB model, the ground state is realized by the superposition of equally weighed dimer configurations, that for doped case is expected to be realized by equal weighted superposition of dimer configurations despite the site occupied by doped fermionic dimers as well. However, due to the antisymmetry of the fermionic dimers, this is only true for at most one doped fermionic dimer. This argument is discussed by J.Feldmeier in [13]. Moreover, the Hamiltonian we obtained for the triangular lattice behaves as the sum of that for square lattice running over three directions. When we later fixed the orientation of doped fermionic dimer, the additional possibility of orientation compared to that on square lattice differs the ground state wave functions. Nevertheless, the deviation can be recovered by adding a diagonal link on square lattice, i.e. a compressed triangular lattice.

3.2 Exact ground states

To examine the exact ground state wave functions of our model, we start in this section with applying the Hamiltonian to a general expansion form of dimer configurations with two doped fermionic dimers, then we detail the expansion form by minimizing

the Hamiltonian. The ground state of arbitrary doping density is finally achieved by a straightforward generalization.

Firstly, we define the three states in following Sec.(3.2.1) and Sec.(3.2.2), and finish the calculations later in Sec.(3.2.3).

3.2.1 Two doped fermionic dimers state

To build up the form of the ground state for two doped fermionic dimers, the discussion in Sec.(3.1.2) suggests that the plausible form of ground state is related to an equally weighed superposition of all dimer configurations. Moreover, the specific form of the Eq.(9) guarantees the Hamiltonian to be positive definite, which implies the zero eigenvalue of Hamiltonian at ground state $|\psi_0\rangle$. In the original RK model, the consistency of these two properties is straightforward to be checked. We define our basic form of doped states

$$|(i_1, \eta_1), (i_2, \eta_2)\rangle \equiv \mathcal{N} \cdot F_{i_1, \eta_1}^\dagger F_{i_2, \eta_2}^\dagger |0\rangle_{(i_1, \eta_1), (i_2, \eta_2)} \otimes \left\{ \sum_{c \in \mathcal{C}_{(i_1, \eta_1), (i_2, \eta_2)}} |c\rangle \right\}, \quad (10)$$

where the zero eigenvalue of H_{RK} is realized by summing up all possible configurations $|c\rangle$ of bosonic dimer on undoped sites equally.

The term \mathcal{N} in Eq.(10) intends to normalize the summation term. We consider that for an N sites lattice with N_t possible configurations in total, the normalized factor gains the form $\mathcal{N} \equiv \sqrt{N_{(i_1, \eta_1), (i_2, \eta_2)} / N_t}$ where $N_{(i_1, \eta_1), (i_2, \eta_2)}$ is the possible configuration of bosonic dimers after doping fermionic dimers on $(i_1, \eta_1), (i_2, \eta_2)$. Thus,

$$\langle (i_1, \eta_1), (i_2, \eta_2) | (i_1, \eta_1), (i_2, \eta_2) \rangle = \frac{N_{(i_1, \eta_1), (i_2, \eta_2)}}{N_t}. \quad (11)$$

In [13], this factor \mathcal{N} is further identified as the classical dimer correlation function Q_c , which yields a vanishing norm $Q_c[c] = 0$ as any QDM-constraint violating configuration c .

3.2.2 Plaquette states

The state of dimers is defined by their locating site as well as their orientations. We use the same indices to characterize the doped fermionic dimers. And since the three

different orientated plaquettes can be assigned to one site, we thus define the plaquette states solely labeled by site l as

$$|\phi_l\rangle = \sum_{\alpha} |\phi_{l,\alpha}\rangle = |\phi_{l,1}\rangle + |\phi_{l,2}\rangle + |\phi_{l,3}\rangle, \quad (12)$$

where the state of certain orientated plaquette e.g. $\alpha = 1$ is

$$|\phi_{l,1}\rangle = F_{i,x}^{\dagger} D_{i+z,x}^{\dagger} + D_{i,x}^{\dagger} F_{i+z,x}^{\dagger} - F_{i,z}^{\dagger} D_{i+x,z}^{\dagger} - D_{i,z}^{\dagger} F_{i+x,z}^{\dagger}. \quad (13)$$

As claimed in Eq.(9), we rewrite the Hamiltonian as a sum of projectors by setting a proper RK line. Note that the projectors of $H_1 + H_{\nu_1}$ part in the Hamiltonian consist of projection operators coinciding with the above defined plaquette states. We then define the projector on site l

$$\begin{aligned} P_l &= P_{l,1} \oplus P_{l,2} \oplus P_{l,3} \\ &= (|\phi_{l,1}\rangle\langle\phi_{l,1}| + |\phi_{l,2}\rangle\langle\phi_{l,2}| + |\phi_{l,3}\rangle\langle\phi_{l,3}|) \otimes \prod_{p \neq l} \mathbb{1}_p \end{aligned} \quad (14)$$

and rewrite the $H_1 + H_{\nu_1}$ part as

$$\begin{aligned} H_1 + H_{\nu_1} &= \sum_l P_l \\ &= \sum_l \sum_{\alpha}^3 P_{l,\alpha} \end{aligned} \quad (15)$$

We finally define a mix state

$$|\phi_{l,\alpha}(i,\eta)\rangle = \frac{1}{\sqrt{N_{(l,\tau),(l+\mu,\tau),(i,\eta)}}} F_{i,\eta}^{\dagger} |0\rangle_{(i,\eta)} \otimes |\phi_{l,\alpha}\rangle \otimes \left\{ \sum_{c \in \mathcal{C}_{(l,\tau),(l+\mu,\tau),(i,\eta)}} |c\rangle \right\}, \quad (16)$$

which is normalized by $1/\sqrt{N_{(l,\tau),(l+\mu,\tau),(i,\eta)}}$, the number of configurations of dimers when the plaquette $|\phi_{l,\alpha}\rangle$ occupy the sites $(l,\tau), (l+\mu,\tau)$ and the doped fermionic dimer is located on (i,η) .

3.2.3 Exact ground state

For the system with only two doped fermionic dimers, we start with the ansatz

$$|\phi_0\rangle = \sum_{i_1, \eta_1, i_2, \eta_2} A_{(i_1, \eta_1), (i_2, \eta_2)} |(i_1, \eta_1), (i_2, \eta_2)\rangle, \quad (17)$$

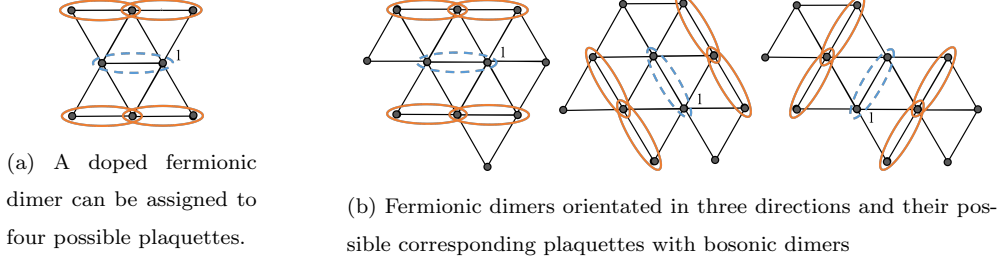


Figure 6: For each doped dimer, four nearby plaquettes are affected by applying Hamiltonian.

i.e. expand the assumed ground state $|\phi_0\rangle$ in terms of the basis functions Eq.(10) with two doped fermionic dimers, and weigh the states with $A_{(i_1,\eta_1),(i_2,\eta_2)}$. Then we apply the Hamiltonian H

$$\begin{aligned}
H|\phi_0\rangle &= J \sum_{\text{plaq}} H_{RK} |\phi_{RK_0}\rangle + \nu_1 \sum_l \sum_{\alpha} \sum_{i_1,\eta_1,i_2,\eta_2}^3 A_{(i_1,\eta_1),(i_2,\eta_2)} P_{l,\alpha} |(i_1,\eta_1), (i_2,\eta_2)\rangle \\
&= \nu_1 \sum_l \sum_{\alpha} \sum_{i_1,\eta_1,i_2,\eta_2}^3 A_{(i_1,\eta_1),(i_2,\eta_2)} P_{l,\alpha} |(i_1,\eta_1), (i_2,\eta_2)\rangle.
\end{aligned} \tag{18}$$

The fact that the RK term vanishes is resulted from the equally weighed bosonic dimer configurations in Eq.(10).

We now observe how the projector $P_{l,\alpha}$ acts on the plaquettes explicitly. It acts non-trivially only on the plaquettes containing a single fermionic dimer. As shown in Fig.(6), one fermionic dimer can be contained by four nearby different orientated plaquettes which are assigned to three labeling sites l . Since the doped dimers are characterized by both its locating site i and orientation η , we apply the projectors with respect to their locating label l as well and treat different orientated dimer separately.

For fermionic dimer located on (i_1, x) ,

$$\begin{aligned}
\sum_{\alpha} P_{l,\alpha} |(i_1, x), (i_2, \eta_2)\rangle &= (P_{l,1} \oplus P_{l,2} \oplus P_{l,3}) |(i_1, x), (i_2, \eta_2)\rangle \\
&= (\delta_{l,i_1} + \delta_{l-x,i_1} + \delta_{l+z,i_1}) P_l |(i_1, x), (i_2, \eta_2)\rangle,
\end{aligned} \tag{19}$$

where for δ_{l,i_1}

$$\begin{aligned}
\delta_{l,i_1}(P_{l,1} \oplus P_{l,2} \oplus P_{l,3})|(i_1, x), (i_2, \eta_2)\rangle &= \delta_{l,i_1}P_{l,\eta_1}|(i_1, x), (i_2, \eta_2)\rangle = \\
&= \frac{1}{\sqrt{N_t}} \sum_{c \in \mathcal{C}_{(l,\eta_1),(i_2,\eta_2)}} |\phi_{l,1}\rangle \langle \phi_{l,1}| F_{l,x}^\dagger F_{i_2,\eta_2}^\dagger (|0\rangle_{(l,x),(i_2,\eta_2)} \otimes |c\rangle). \tag{20}
\end{aligned}$$

To further simplify this expression, we take one bosonic dimer from $|c\rangle$ and combine it with the fermionic dimer $F_{l,x}^\dagger$ from before into a plaquette state coupling with $\langle \phi_{l,1}|$:

$$\begin{aligned}
&= \frac{1}{\sqrt{N_t}} \sum_{c \in \mathcal{C}_{(l,x),(i_2,\eta_2)}} |\phi_{l,1}\rangle \langle \phi_{l,1}| F_{l,x}^\dagger F_{i_2,\eta_2}^\dagger (|0\rangle_{(l,x),(i_2,\eta_2)} \otimes |c\rangle) = \\
&= \frac{1}{\sqrt{N_t}} \sum_{c' \in \mathcal{C}_{(l,x),(i_2,\eta_2),(l+z,x)}} |\phi_{l,1}\rangle \langle \phi_{l,1}| F_{l,x}^\dagger F_{i_2,\eta_2}^\dagger D_{l+z,x}^\dagger (|0\rangle_{(l,x),(i_2,\eta_2),(l+z,x)} \otimes |c'\rangle) = \\
&= \frac{1}{\sqrt{N_t}} \langle \phi_{l,1}| F_{l,x}^\dagger D_{l+z,x}^\dagger |0\rangle_{(l,x),(l+z,x)} F_{i_2,\eta_2}^\dagger |0\rangle_{(i_2,\eta_2)} \otimes |\phi_{l,1}\rangle \otimes \left\{ \sum_{c' \in \mathcal{C}_{(l,x),(i_2,\eta_2),(l+z,x)}} |c'\rangle \right\} = \\
&= \langle \phi_{l,1}| F_{l,x}^\dagger D_{l+z,x}^\dagger |0\rangle_{(l,x),(l+z,x)} \sqrt{\frac{N_{(l,\tau),(l+\mu,\tau),(i,\eta)}}{N_t}} \otimes F_{i_2,\eta_2}^\dagger |0\rangle_{(i_2,\eta_2)} \otimes |\phi_{l,1}\rangle = \\
&= \langle \phi_{l,1}| F_{l,x}^\dagger D_{l+z,x}^\dagger |0\rangle_{(l,x),(l+z,x)} \sqrt{Q_c[(l,x), (l+z,x), (i_2, \eta_2)]} |\phi_{l,1}, (i_2, \eta_2)\rangle \\
&= +\sqrt{Q_c[(l,x), (l+z,x), (i_2, \eta_2)]} |\phi_{l,1}, (i_2, \eta_2)\rangle. \tag{21}
\end{aligned}$$

Analogously, we can repeat the calculation for other kronecker deltas as well as orientations:

$$\begin{aligned}
(\delta_{l,i_1} + \delta_{l-x,i_1} + \delta_{l+z,i_1})P_l|(i_1, x), (i_2, \eta_2)\rangle &= \\
&+ \delta_{l,i_1} \sqrt{Q_c[(l,x), (l+z,x), (i_2, \eta_2)]} |\phi_{l,1}, (i_2, \eta_2)\rangle \\
&- \delta_{l-x,i_1} \sqrt{Q_c[(l,x), (l+y,x), (i_2, \eta_2)]} |\phi_{l,2}, (i_2, \eta_2)\rangle \\
&+ \delta_{l+z,i_1} \sqrt{Q_c[(l,x), (l-z,x), (i_2, \eta_2)]} |\phi_{l,1}, (i_2, \eta_2)\rangle \\
&- \delta_{l+z,i_1} \sqrt{Q_c[(l,x), (l-y,x), (i_2, \eta_2)]} |\phi_{l,2}, (i_2, \eta_2)\rangle \tag{22}
\end{aligned}$$

$$\begin{aligned}
(\delta_{l,i_1} + \delta_{l-y,i_1} + \delta_{l-x,i_1})P_l|(i_1, y), (i_2, \eta_2)\rangle = & \\
& + \delta_{l,i_1} \sqrt{Q_c[(l, y), (l-x, y), (i_2, \eta_2)]} |\phi_{l,2}, (i_2, \eta_2)\rangle \\
& - \delta_{l-y,i_1} \sqrt{Q_c[(l, y), (l+z, y), (i_2, \eta_2)]} |\phi_{l,3}, (i_2, \eta_2)\rangle \\
& + \delta_{l-x,i_1} \sqrt{Q_c[(l, y), (l+x, y), (i_2, \eta_2)]} |\phi_{l,2}, (i_2, \eta_2)\rangle \\
& - \delta_{l-x,i_1} \sqrt{Q_c[(l, y), (l-z, y), (i_2, \eta_2)]} |\phi_{l,3}, (i_2, \eta_2)\rangle
\end{aligned} \tag{23}$$

$$\begin{aligned}
(\delta_{l,i_1} + \delta_{l-y,i_1} + \delta_{l+x,i_1})P_l|(i_1, z), (i_2, \eta_2)\rangle = & \\
& + \delta_{l,i_1} \sqrt{Q_c[(l, z), (l-y, z), (i_2, \eta_2)]} |\phi_{l,3}, (i_2, \eta_2)\rangle \\
& - \delta_{l,i_1} \sqrt{Q_c[(l, z), (l+x, z), (i_2, \eta_2)]} |\phi_{l,1}, (i_2, \eta_2)\rangle \\
& + \delta_{l-y,i_1} \sqrt{Q_c[(l, z), (l+y, z), (i_2, \eta_2)]} |\phi_{l,3}, (i_2, \eta_2)\rangle \\
& - \delta_{l+x,i_1} \sqrt{Q_c[(l, z), (l-x, z), (i_2, \eta_2)]} |\phi_{l,1}, (i_2, \eta_2)\rangle.
\end{aligned} \tag{24}$$

Fig.(6b) illustrates the above presented results, where each orientated fermionic dimer has four coupling bosonic dimers. They are combined together so that four mix states with alternating sign are generated. In the next step, we insert previous results into Eq.(18) and obtain

$$\begin{aligned}
& \sum_l \sum_{i_1, \eta_1, i_2, \eta_2} A_{(i_1, \eta_1), (i_2, \eta_2)} P_l |(i_1, \eta_1), (i_2, \eta_2)\rangle = \\
& \sum_{l, \eta_1, i_2, \eta_2} A_{(i_1, \eta_1), (i_2, \eta_2)} [(\delta_{l,i_1} \sqrt{Q_c[(l, x), (l+z, x), (i_2, \eta_2)]} + \delta_{l+z, i_1} \sqrt{Q_c[(l, x), (l-z, x), (i_2, \eta_2)]} \\
& \quad - \delta_{l,i_1} \sqrt{Q_c[(l, z), (l+x, z), (i_2, \eta_2)]} - \delta_{l+x, i_1} \sqrt{Q_c[(l, z), (l-x, z), (i_2, \eta_2)]}] |\phi_{l,1}, (i_2, \eta_2)\rangle \\
& \quad (-\delta_{l-x, i_1} \sqrt{Q_c[(l, x), (l+y, x), (i_2, \eta_2)]} - \delta_{l+z, i_1} \sqrt{Q_c[(l, x), (l-y, x), (i_2, \eta_2)]} \\
& \quad + \delta_{l,i_1} \sqrt{Q_c[(l, y), (l-x, y), (i_2, \eta_2)]} + \delta_{l-x, i_1} \sqrt{Q_c[(l, y), (l+x, y), (i_2, \eta_2)]}] |\phi_{l,2}, (i_2, \eta_2)\rangle \\
& \quad (-\delta_{l-y, i_1} \sqrt{Q_c[(l, y), (l+z, y), (i_2, \eta_2)]} - \delta_{l-x, i_1} \sqrt{Q_c[(l, y), (l-z, y), (i_2, \eta_2)]} \\
& \quad + \delta_{l,i_1} \sqrt{Q_c[(l, z), (l-y, z), (i_2, \eta_2)]} + \delta_{l-y, i_1} \sqrt{Q_c[(l, z), (l+y, z), (i_2, \eta_2)]}] |\phi_{l,3}, (i_2, \eta_2)\rangle] \\
& + \sum_{i_1, \eta_1, l, \eta_2} [\dots] |(i_1, \eta_1), \phi_l\rangle
\end{aligned} \tag{25}$$

As J.Feldmeier argued in [13], the classical correlation function $Q_c[(l, \eta), (l+\mu, \eta), (i_2, \eta_2)]$ does not have true dependence on η and μ . Moreover, as claimed in Sec.(3.1.2), the Hamiltonian is expected to have minimal value at zero, we consequently demand the coefficient for each term to vanish. It turns out that the coefficient $A_{(i_1, \eta_1), (i_2, \eta_2)}$ is constrained with conditions

$$\begin{aligned}
A_{(l,x),(i_2,\eta_2)} + A_{(l+z,x),(i_2,\eta_2)} - A_{(l,z),(i_2,\eta_2)} - A_{(l+x,z),(i_2,\eta_2)} &= 0 \\
A_{(l-x,y),(i_2,\eta_2)} + A_{(l,y),(i_2,\eta_2)} - A_{(l+z,x),(i_2,\eta_2)} - A_{(l-x,x),(i_2,\eta_2)} &= 0 \\
A_{(l-y,z),(i_2,\eta_2)} + A_{(l,z),(i_2,\eta_2)} - A_{(l-y,y),(i_2,\eta_2)} - A_{(l-x,y),(i_2,\eta_2)} &= 0
\end{aligned} \tag{26}$$

and symmetrical conditions for (i_2, η_2) .

To solve these conditions, we employ the ansatz

$$A_{(i_1, \eta_1), (i_2, \eta_2)} = a_{i_1, \eta_1} a_{i_2, \eta_2}, \tag{27}$$

and insert it into Eq.(26). It yields three equalities

$$\begin{aligned}
a_{(l_m,x),(i_2)} + a_{(l_m+z,x)} - a_{(l_m,z)} - a_{(l_m+x,z)} &= 0 \\
a_{(l_m-x,y)} + a_{(l_m,y)} - a_{(l_m+z,x)} - a_{(l_m-x,x)} &= 0 \\
a_{(l_m-y,z)} + a_{(l_m,z)} - a_{(l_m-y,y)} - a_{(l_m-x,y)} &= 0
\end{aligned} \tag{28}$$

for $m = 1, 2$. Hence, for more doped fermionic dimers $m = 1, \dots, N_f$, the conditions are easily expanded as for each dimer they are mutually independent. By introducing the lattice momenta \mathbf{p}_m , we make the ansatz

$$a_{i_m, \eta_m} = a_{i_m, \eta_m}(\mathbf{p}_m) = C_{\eta_m}(\mathbf{p}_m) e^{i\mathbf{p}_m \cdot \mathbf{i}_m}. \tag{29}$$

The exact ground state with two doped dimers is

$$|\phi_0\rangle = \sum_{i_1, \eta_1, i_2, \eta_2} a_{i_1, \eta_1}(\mathbf{p}_1) a_{i_2, \eta_2}(\mathbf{p}_2) |(i_1, \eta_1), (i_2, \eta_2)\rangle = |\mathbf{p}_1, \mathbf{p}_2\rangle, \tag{30}$$

namely the exact ground state is characterized by the lattice momentum of doped dimers, which can be directly generalized to arbitrary fermion number. By inserting Eq.(29) into conditions Eq.(28), we obtain

$$C_x(\mathbf{p}_m) = C_z(\mathbf{p}_m) \frac{1 + e^{i\mathbf{p}_m \cdot \mathbf{x}}}{1 + e^{i\mathbf{p}_m \cdot \mathbf{z}}} \tag{31}$$

and

$$C_y(\mathbf{p}_m) = C_x(\mathbf{p}_m) \frac{1 + e^{ip_m,y}}{1 + e^{ip_m,x}} = C_z(\mathbf{p}_m) \frac{1 + e^{ip_m,y}}{1 + e^{ip_m,z}} \quad (32)$$

as on the triangular lattice the sum of unit vectors $\mathbf{x} + \mathbf{z}$ reproduces the unit vector \mathbf{y} . Finally, with the normalization $|C_x|^2 + |C_x|^2 + |C_x|^2 = \frac{9}{N}$ of Eq.(30), where 9 comes from 3×3 possibilities of orientations for two doped fermionic dimers, $C_\eta(\mathbf{p}_m)$ has the choice:

$$C_\eta = \frac{3}{\sqrt{N}} \frac{1 + e^{ip_m,\eta}}{\sqrt{|1 + e^{ip_m,x}|^2 + |1 + e^{ip_m,y}|^2 + |1 + e^{ip_m,z}|^2}}, \quad (33)$$

which has a similar form compared to the choice of C_η on square lattice in [13]: we add a normalization term representing y -direction orientated momenta into the denominator, and replace the number of orientations 2 on the square lattice with 3. The relationships among C_η indicated this result already as well. By taking one orientation of plaquette on the triangular lattice away, we can reproduce the choice made for square lattice. On the other hand, our anticipation in Sec.(3.2.1) is confirmed that a triangular case can be recovered by adding the diagonal orientation into square lattice.

3.3 Perturbations around RK line

We further proceed the study of perturbations in the parameter space, which is expected to change the ground state structure thoroughly. It suggests that the deviations around RK line lead to a dispersion relation of energy and lattice momenta in contrary to the huge degeneracy of the ground state. In accordance with the work done by J.Feldmerier in [13], we do following calculations to investigate the perturbed energy. We start in a like manner with two doped dimers and restrict the perturbations in exchange hopping parameters t_1 and t_3 . With the first order perturbation, we evaluate the energy by determining

$$E = E_0 + \langle \mathbf{p}_1 \mathbf{p}_2 | \Delta H_{t_i} | \mathbf{p}_1 \mathbf{p}_2 \rangle = \langle \mathbf{p}_1 \mathbf{p}_2 | \Delta H_{t_i} | \mathbf{p}_1 \mathbf{p}_2 \rangle, \quad (34)$$

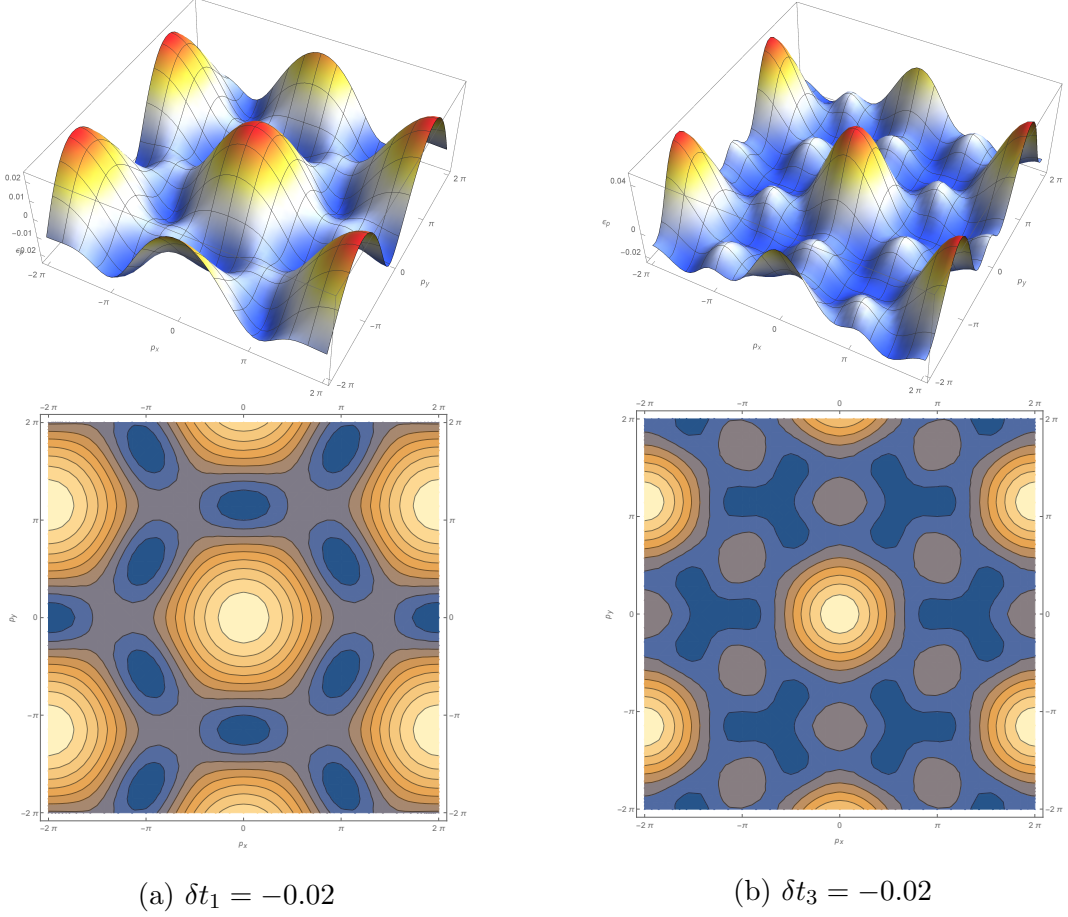


Figure 7: The dispersion relation for $\delta t_1 = -0.02$, $J = V = 1$.(a)(b) show that small perturbations around RK-Line change the ground state dramatically and Fermi pockets emerge already at the edge of first Brillouin zone.

where

$$\Delta H_{t_i} = -\delta t_i \sum_{s=1}^{S_{t_i}} \sum_{j,\eta} F_{j+r_{t_i}^{s,\eta},\eta+\eta_{t_i}}^\dagger D_{j,\eta}^\dagger D_{j+r_{t_i}^{s,\eta},\eta+\eta_{t_i}} F_{j,\eta}. \quad (35)$$

In the second equality, we merely summarize the Hamiltonian in Eq.(9) by introducing the displacement vector $r_{t_i}^{s,\eta}$, changing of the orientation η_{t_i} and then summing up S_{t_i} correlated terms referring to the given interaction process t_i . Additionally, t_i is replaced by its deviation δt_i to associate with perturbation.

We then insert Eq.(17) into Eq.(35) and (34) in order to identify the expression of

$\Delta E(\mathbf{p}_1 \mathbf{p}_2)$:

$$\begin{aligned} \Delta E = & -\delta t_i \sum_{s=1}^{S_{t_i}} \sum_{j,\eta} \sum_{i_1, \eta_1, i_2, \eta_2} \sum_{l_1, \tau_1, l_2, \tau_2} a_{i_1, \eta_1}(\mathbf{p}_1) a_{i_2, \eta_2}(\mathbf{p}_2) a_{l_1, \tau_1}^*(\mathbf{p}_1) a_{l_2, \tau_2}^*(\mathbf{p}_2) \times \\ & \times \langle (l_1, \tau_1), (l_2, \tau_2) | F_{j+r_{t_i}^s, \eta, \eta+\eta_{t_i}}^\dagger D_{j,\eta}^\dagger D_{j+r_{t_i}^s, \eta, \eta+\eta_{t_i}} F_{j,\eta} | (i_1, \eta_1), (i_2, \eta_2) \rangle. \end{aligned} \quad (36)$$

With an universe evaluation of the matrix element done by Federmeier in [13] and the abbreviation $i_1 = (i_1, \eta_1)$ he used, we thus obtain

$$\begin{aligned} \Delta E = & -\delta t_i \sum_{s=1}^{S_{t_i}} \sum_{i_1, i_2} t_i (a_{i_1}(\mathbf{p}_1) a_{i_2}(\mathbf{p}_2) a_{i_1+r_{t_i}^s, i_1}^*(\mathbf{p}_1) a_{i_2}^*(\mathbf{p}_2) - a_{i_1}(\mathbf{p}_1) a_{i_2}(\mathbf{p}_2) a_{i_1+r_{t_i}^s, i_1}^*(\mathbf{p}_2) a_{i_2}^*(\mathbf{p}_1)) \times \\ & \times Q_c[i_1, i_2, i_1 + r^s, i_1] + \\ & + \delta t_i (\dots) \times Q_c[i_1, i_2, i_2 + r^s, i_2]. \end{aligned} \quad (37)$$

Note that it can be written as a sum of single particle energy $\sum_{\mathbf{p}_i} \epsilon_{\mathbf{p}_i}$ if we only consider the leading order in low doping limit, since the cross coefficients, e.g. in the first term, $a_{i_2}(\mathbf{p}_2) a_{i_2}^*(\mathbf{p}_2)$ can be evaluated together as a constant, and the left part has the variable \mathbf{p}_1 only. By inserting 29 into the leading order terms, the single particle energy is thus defined as:

$$\epsilon(\mathbf{p}_i) \equiv -\delta t_i \sum_{\eta_i} \frac{(1 + e^{i\mathbf{p}_i, \eta_i})(1 + e^{-i\mathbf{p}_i, \eta_i + \eta_{t_i}})}{|1 + e^{ip_{m,x}}|^2 + |1 + e^{ip_{m,y}}|^2 + |1 + e^{ip_{m,z}}|^2} \sum_{s=1}^{S_{t_i}} [e^{-ir_{t_i}^s, \eta_i \cdot \mathbf{p}_i}] Q_c[(0, \eta_i) | r_{t_i}^s, \eta_i], \quad (38)$$

whose dispersion in momenta space is illustrated in Fig.(7).

4 Summary

Here we briefly summarize our previous calculations. Our goal is to expand QDM onto the triangular lattice. To examine the explicit form of Hamiltonian and the ground states, we follow the calculations on the square lattice in [13] and adapt them according to the specific geometry of the triangular lattice. We start with building up the Hamiltonian, then follow the method proposed by Rokhsar and Kivelson to rewrite the Hamiltonian into exact solvable form at chosen parameter line. Based on it we obtain the exact ground state which confirmed our expectations.(Sec.3.2.3) From [13] we know that small perturbations around exactly solvable parameter line lead to a collapse of the flat energy band in momentum space. Consequently a non-trivial dispersion relation emerges, where the significant structure Fermi pocket can be observed. These conclusions are recovered in the triangular lattice case as well. As shown in Fig.(7), the dispersion relation is apparently distinct from flat band at very small perturbations ($t_i = -0.02$), and small tunnels appear at the edge of the first Brillouin zone.

For further study of QDM in the triangular lattice, the states $|\mathbf{p}_1, \dots, \mathbf{p}_{N_f}\rangle$ is expected to reconstructed with creation and annihilation operators which fulfill canonical fermionic anticommutation relations as in square lattice case. Finally, a fractionalized Fermi liquid structure (FL*) is able to be built upon the triangular lattice.

References

- ¹J. M. Bednorz, “Fractionalized fermi liquids”, *Z.Phys B - Condensed Matter* **64**, 216403 (189–193).
- ²H. Alloul, T. Ohno, and P. Mendels, “⁸⁹Y nmr evidence for a fermi-liquid behavior in $\text{yba}_2\text{cu}_3\text{o}_6 + x$ ”, *Phys. Rev. Lett.* **63**, 1700–1703 (1989).
- ³J. W. Loram, K. A. Mirza, J. R. Cooper, and W. Y. Liang, “Electronic specific heat of $\text{yba}_2\text{cu}_3\text{o}_6 + x$ from 1.8 to 300 k”, *Phys. Rev. Lett.* **71**, 1740–1743 (1993).
- ⁴J. Loram, J. Luo, J. Cooper, W. Liang, and J. Tallon, “Evidence on the pseudogap and condensate from the electronic specific heat”, *Journal of Physics and Chemistry of Solids* **62**, 59–64 (2001).
- ⁵P. A. Lee, N. Nagaosa, and X.-G. Wen, “Doping a mott insulator: physics of high-temperature superconductivity”, *Rev. Mod. Phys.* **78**, 17–85 (2006).
- ⁶M. Punk, A. Allais, and S. Sachdev, “Quantum dimer model for the pseudogap metal”, *Proceedings of the National Academy of Sciences* **112**, 9552–9557 (2015).
- ⁷H.-B. Yang, J. D. Rameau, Z. Pan, G. D. Gu, P. D. Johnson, H. Claus, D. Hinks, and T. E. Kidd, “Reconstructed fermi surface of underdoped $\text{bi}_2\text{sr}_2\text{cacu}_2\text{o}_{8+}$ cuprate superconductors.”, *Physical review letters* **107** 4, 047003 (2011).
- ⁸K. M. Shen, F. Ronning, D. H. Lu, F. Baumberger, N. J. C. Ingle, W. S. Lee, W. Meevasana, Y. Kohsaka, M. Azuma, M. Takano, H. Takagi, and Z.-X. Shen, “Nodal quasiparticles and antinodal charge ordering in $\text{ca}_2\text{-xnaxcu}_2\text{cl}_2$ ”, *Science* **307**, 901–904 (2005).
- ⁹Y. Ando, Y. Kurita, S. Komiya, S. Ono, and K. Segawa, “Evolution of the hall coefficient and the peculiar electronic structure of the cuprate superconductors”, *Phys. Rev. Lett.* **92**, 197001 (2004).
- ¹⁰S. Badoux, W. Tabis, F. Laliberté, G. Grissonnanche, B. Vignolle, D. Vignolles, J. Béard, D. Bonn, W. Hardy, R. Liang, et al., “Change of carrier density at the pseudogap critical point of a cuprate superconductor”, *Nature* **531**, 210 (2016).

- ¹¹S. Uchida and T. Ido, “S. uchida, t. ido, h. takagi, t. arima, y. tokura, and s. tajima, phys. rev. b 43, 7942 (1991).”, Phys. Rev. B **43**, 7942 (1991).
- ¹²T. Senthil, S. Sachdev, and M. Vojta, “Fractionalized fermi liquids”, Phys. Rev. Lett. **90**, 216403 (2003).
- ¹³J. Feldmeier, “Spectral functions and exact solutions in a quantum dimer model for pseudogap metals”, (2018).
- ¹⁴D. S. Rokhsar and S. A. Kivelson, “Superconductivity and the quantum hard-core dimer gas”, Phys. Rev. Lett. **61**, 2376–2379 (1988).
- ¹⁵P. W. ANDERSON, “The Resonating Valence Bond State in La₂CuO₄ and Superconductivity”, Science **235**, 1196–1198 (1987).
- ¹⁶S. A. Kivelson, D. S. Rokhsar, and J. P. Sethna, “Topology of the resonating valence-bond state: solitons and high- T_c superconductivity”, Phys. Rev. B **35**, 8865–8868 (1987).
- ¹⁷R. Moessner and S. L. Sondhi, “Resonating valence bond liquid physics on the triangular lattice”, Progress of Theoretical Physics Supplement **145**, 37–42 (2002).
- ¹⁸R. K. Moessner R., “Quantum dimer models”, Introduction to Frustrated Magnetism **164**, 437–479 (2011).
- ¹⁹R. Moessner and S. L. Sondhi, “Resonating valence bond phase in the triangular lattice quantum dimer model”, Phys. Rev. Lett. **86**, 1881–1884 (2001).